

## Synthesis, Optical and Thermal Properties of $\beta$ -Alanine $\beta$ -Alaninium Picrate Single Crystal

A.Thirugnanam<sup>1</sup>, and P.Praveen Kumar<sup>1\*</sup>

<sup>1</sup>Department of Physics, Presidency College, Chennai-5, Tamilnadu. India.

\*ppkpresidency@gmail.com

---

**ABSTRACT:** The organic nonlinear optical (NLO) material  $\beta$ -Alanine  $\beta$ -Alaninium Picrate ( $\beta$ -AAP) was grown by slow evaporation technique. Powder X-ray diffraction patterns were recorded and indexed for further confirmation of crystalline nature of grown ( $\beta$ -AAP) crystal. The transparent range of the grown material was studied using UV-Vis-NIR spectral analysis and the optical band gap was evaluated from the absorption spectrum. The photoluminescence spectra of the grown crystal have been recorded and it shows a high intensity peak at 455 nm. The modes of vibrations of different molecular groups present in the sample were identified using FTIR spectral analysis. Thermal behavior of the crystal has been investigated by DTA and TGA analysis. The surface properties and morphology have been investigated using Scanning Electron Micrograph (SEM). The third-order nonlinear optical parameters for  $\beta$ -AAP single crystal are determined using Z-scan technique.

**Keywords:** Crystal growth, Microhardness, NLO, UV-Vis-NIR, X-ray diffraction.

---

### I. INTRODUCTION

In recent years, nonlinear optical (NLO) crystals have attracted much attention for their large nonlinear coefficient with lower cut-off wavelength and high laser damage threshold. The search and design of high efficient NLO crystals for visible and UV region are very important for laser processing and photonics devices, optical communication, optical storage devices and numerous device applications [1, 2]. 3-Aminopropionic acid commonly known as  $\beta$ -alanine with molecular formula  $C_3H_7NO_2$  and in which the amino group is at the  $\beta$ -position from the carboxylate group [3-5]. Supplementation with  $\beta$ -alanine has been shown to increase the concentration of carosine in muscles, decrease in fatigue in athletes and increase total muscular work done.  $\beta$ -alanine is purely a synthetic amino acid and it is a positional isomer of L-alanine [6,7]. It forms crystalline complexes with organic, inorganic acids or salts.

The picric acid complexes possess higher molecular polarizability due to the transfer of proton than the nonlinear optical crystals [8]. Picric acid (2, 4, 6-trinitrophenol) is an organic acid, which is used, in the dyeing industry and as an explosive. The presence of three electron withdrawing nitro groups makes it as a good  $\pi$ -acceptor for neutral carrier donor molecule [9-11]. The metal derivatives of picric acid are helpful in homeopathy medicine and it shows extraordinary variety in the bonding of metal salts and complexes [12]. Moreover, there have been several spectral analyses done on  $\beta$ -alanine [13, 14] with inorganic acids like nitric, perchloric and sulfuric acids. The importance of picric acid and metal picrate in biomedicine has made the researchers to focus on amino acids crystals of picrate.

In the present study, the title compound  $\beta$ -Alanine  $\beta$ -Alaninium Picrate [ $\beta$ -AAP] crystals were successfully grown by slow evaporation technique. Characterization studies such as Single crystal XRD, Powder X-ray Diffraction, UV-Vis-NIR, FT-IR, TGA and DTA study have been carried out for the grown crystal. SEM and Z-SCAN analysis were also done for the grown  $\beta$ -AAP crystal.

### II. EXPERIMENTAL PROCEDURE

#### 2.1 Crystal Growth

$\beta$ -alanine and picric acid were taken in the 2:1 ratio and dissolved thoroughly in de-ionized water at room temperature. A saturated solution was prepared and the solution was filtered using a Whatmann filter paper. The filtered solution in a beaker was allowed to evaporate by slow evaporation technique. Good yellow colour, transparent single crystals were obtained within a period of 15 - 20 days. The photograph of the grown crystal is shown in Fig 1.

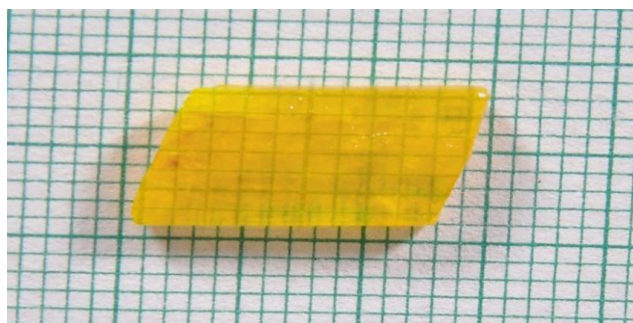


Fig.1. Photograph of the  $\beta$ -AAP crystal.

### III. RESULTS AND DISCUSSION

#### 3.1 Single crystal XRD Analysis

Single crystal X-ray diffraction analysis for the grown crystal has been carried out to identify the lattice parameters using an MESSRS ENRAF NONUS CAD4F single X-ray diffractometer. The lattice parameters of the grown crystal were found to be  $a = 4.9515 (4) \text{ \AA}$ ,  $b = 11.725 (2) \text{ \AA}$ ,  $c = 14.931 (2) \text{ \AA}$ ,  $\alpha = 78.000 (10)^\circ$ ,  $\beta = 83.750 (10)^\circ$ ,  $\gamma = 82.450 (10)^\circ$  and volume  $V = 837.5 (2) \text{ \AA}^3$ . From the XRD data it is absorbed that the grown  $\beta$ -AAP crystal belongs to triclinic system with the space group  $P\bar{1}$ .

#### 3.2 Powder X-ray Diffraction Studies

Powder X-ray diffraction has been carried out using a XPERT-PRO X-ray diffractometer with  $\text{CuK}\alpha$  ( $\lambda = 1.54056 \text{ \AA}$ ) radiation. The sample was scanned over the range of  $10^\circ - 70^\circ$  at a rate of  $2^\circ/\text{min}$ . The recorded powder X-ray diffraction pattern for  $\beta$ -AAP crystal is shown in Fig.2. The diffraction peaks were indexed using PROZSKI software for the determined values of lattice parameters. The sharp and well defined peaks indicate the crystalline nature of the compound.

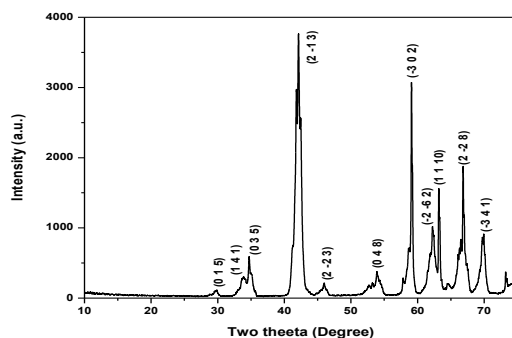


Fig. 2. Powder XRD spectrum of the  $\beta$ -AAP crystal.

#### 3.3 UV-Vis-NIR Analysis

The optical properties of the crystals are important and they provide the information on the electronic band structures, localized states and types of optical transitions. The UV – visible transmittance spectrum of the grown crystal was recorded in the wavelength range 200 - 920 nm using Perkin Elmer Lambda 35 spectrometer and is shown in Fig.3. For this study optically transparent, cut and polished single crystal of thickness 2 mm was used. From the graph, it is clear that the  $\beta$ -AAP crystal is highly transparent in the entire visible region. The high transparency of the material suggests its suitability for second harmonic generation and its suitability in optoelectronic devices [15]. The lower cut off wavelength for  $\beta$ -AAP crystal is 455 nm.

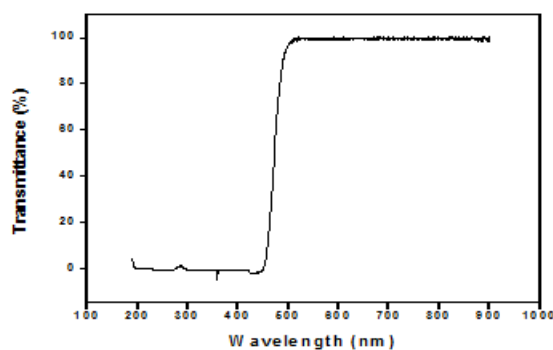


Fig. 3. UV-Vis-NIR spectra of the  $\beta$ -AAP crystal.

### 3.4. Fluorescence Studies

Fluorescence finds wide application in the branches of biochemistry and medicine. It is also used as lighting in fluorescent lamps, Light Emitting Diode (LED) lamps etc. The excitation and emission spectra for  $\beta$ -AAP recorded using FP - 6500 Spectrofluorometer shown in Fig.4. Fluorescence is a form of luminescence in which the light is emitted by a substance that has absorbed light. The emitted light has a longer wavelength and therefore lower energy than the absorbed radiation. Fluorescence is mostly expected in molecules that are aromatic or contain multiple conjugated system double bonds than compounds with aliphatic and alicyclic carbonyl structures. The emission spectrum for  $\beta$ -AAP was recorded using Fluorescence spectrometer. The sample was excited at 360 and 415 nm and the fluorescence emission spectrum was obtained in the range 190 – 900 nm and is depicted in Fig. 4. A peak at 455 nm was observed in the emission spectrum. The results indicate that  $\beta$ -AAP crystals have a blue fluorescence emission. It shows that the  $\beta$ -AAP crystal can be used in nonlinear optical and blue organic light emitting diode applications.

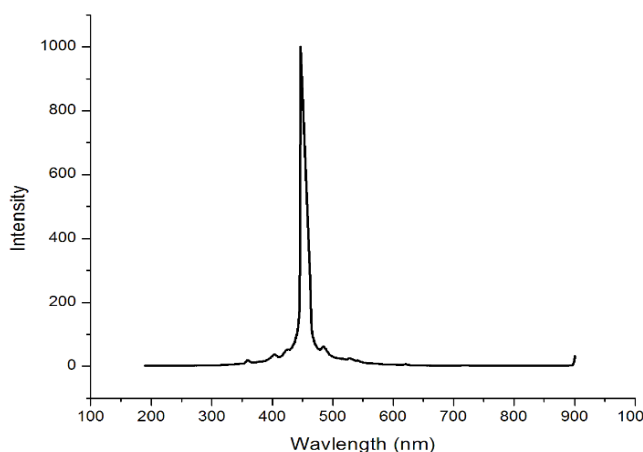


Fig.4. Emission spectrum of the  $\beta$ -AAP crystal.

### 3.5 Determination of optical band gap

The dependence of optical absorption coefficient with the photon energy helps to study the band structure and the type of transition of electron [16]. The optical absorption coefficient ( $\alpha$ ) was calculated from the transmittance using the following relation.

$$\alpha = \frac{1}{t} \log \left( \frac{1}{T} \right) \quad (1)$$

Where T is the transmittance and t is the thickness of the crystal. Owing to the direct band gap, the crystal under study has an absorption coefficient ( $\alpha$ ) obeying the following relation for high photon energies ( $h\nu$ ):

$$\alpha = \frac{A(h\nu - E_g)^{1/2}}{h\nu} \quad (2)$$

Where  $E_g$  is optical band gap of the crystal and A is a constant. The plot of variation of  $(\alpha h\nu)^2$  versus  $h\nu$  is shown in Fig 5 .  $E_g$  is evaluated by the extrapolation of the linear part [17]. The band gap of the  $\beta$ -AAP crystals were found to be 2.1 eV .

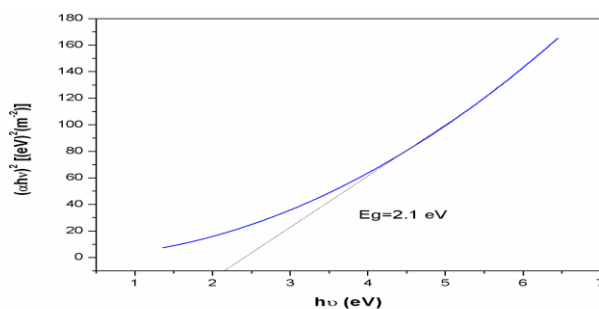


Fig. 5. Plot  $(nh\nu)^2$  Vs  $h\nu$  of the  $\beta$ -AAP crystal.

### 3.6 Fourier Transform Infrared (FT-IR) Analysis

The FT-IR analysis is carried out to analyze the presence of functional groups of the synthesized compound. The FT-IR spectra of  $\beta$ -AAP crystal was recorded at room temperature in the range of  $400\text{ cm}^{-1}$  -  $4000\text{ cm}^{-1}$  by employing BRUKKER IFS 66V FT-IR spectrometer, using KBr pellet method. The FT-IR spectrum of  $\beta$ -AAP crystal is shown in Fig 6. It is evident from the spectrum that the band at  $3419.84\text{ cm}^{-1}$  is assigned to the N-H stretching vibration of primary amine group. The peak at  $3245\text{ cm}^{-1}$  is due to symmetric and asymmetric stretching of  $\text{NH}_2$ . The band observed around  $3083.04\text{ cm}^{-1}$  corresponds to  $\text{NH}_3^+$  stretching frequencies. The C=O stretching vibration was observed in  $1567.42\text{ cm}^{-1}$ . The band at  $1268.64\text{ cm}^{-1}$  is due to the C-O stretching vibration of carboxylic acid group. The peak at  $1152.49\text{ cm}^{-1}$  in the spectrum is assigned to C-O stretching vibration of ester. The C-H stretching vibration bands of the aromatic ring appear are  $794.78$  and  $705\text{ cm}^{-1}$  respectively. The observed vibration wave number of  $\beta$ -AAP crystal is shown in Table 1.

Table-1: FT-IR absorption frequencies of  $\beta$ -AAP crystal.

Wave number ( $\text{cm}^{-1}$ )	Assignment
3419.84	N-H stretching
3245	Symmetric and asymmetric stretching
3083.04	$\text{NH}_3^+$ stretching frequencies
1567.42	C=O stretching
1286.64 & 1152.49	C-O stretching
794.78	C-H bending
705.00	C-H stretching

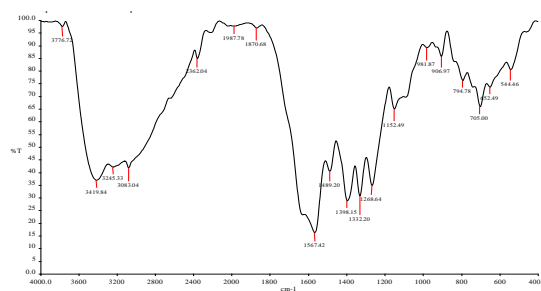


Fig. 6. The FT-IR Spectrum of the  $\beta$ -AAP crystal.

### 3.7 Thermal Studies

The  $\beta$ -AAP crystal was subjected to thermo gravimetric analysis (TGA) and differential thermal analysis (DTA) simultaneously using NETSZCH STA 409°C, in nitrogen atmosphere. The sample was heated at a rate of  $25^\circ\text{ C/min}$ . From the TG curve it is inferred that the sample of the title crystal undergoes decomposition in four stages. The compound is stable up to  $185^\circ\text{ C}$ . In the first stage, only 1.63 % weight loss is observed in the temperature range  $185^\circ\text{ C} - 280^\circ\text{ C}$ . In the second stage, a weight loss of 50.22% is observed in the temperature range  $280^\circ\text{ C} - 420^\circ\text{ C}$ . In the third stage, a weight loss of 11.60% is observed in the temperature range  $420^\circ\text{ C} - 540^\circ\text{ C}$ . In the final stage, a weight loss of 6.80% is observed in the temperature range  $540^\circ\text{ C} - 700^\circ\text{ C}$ . The weight loss in each stage is due to the liberation of gaseous products. The residual mass of 33% may be due to the presence of carbon in the remaining decomposed material. The DTA curve indicates an endothermic peak at  $148.5^\circ\text{ C}$  corresponds to the melting point of the crystal.

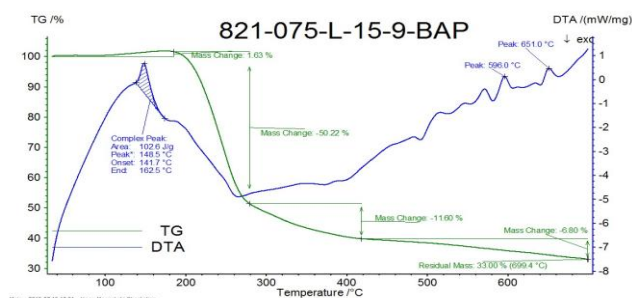


Fig. 7. TG-DTA curves of the  $\beta$ -AAP crystal.

### 3.8. SEM analysis

The surface morphology and dislocation on the surface of the grown crystal was magnified and analyzed using JSM 840-A scanning electron microscope. The transparent growth plane of  $\beta$ -AAP crystal was coated with gold to discharge the charge of particles and at four different magnifications is shown in Fig. 8.a & Fig. 8.b. From the image, it is clear that  $\beta$ -AAP crystal possesses relatively smooth surface and the presence of different kinds of atoms present in the grown material.

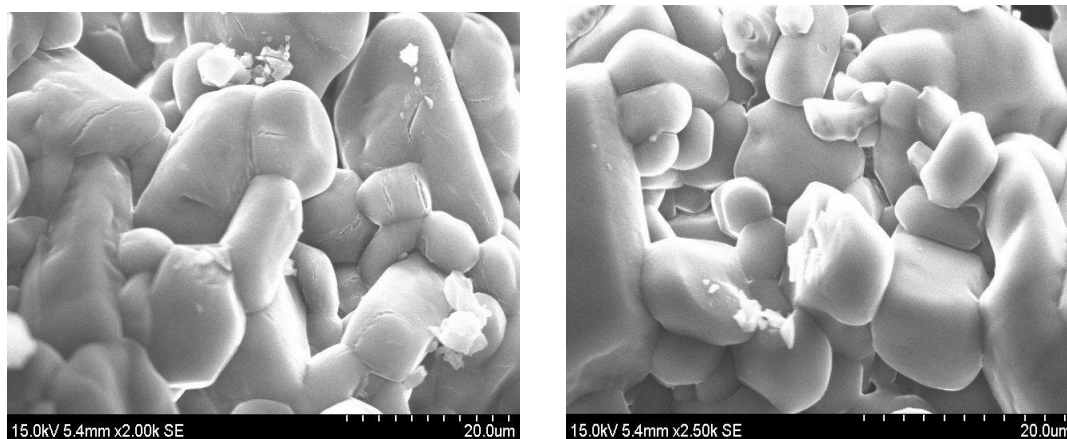


Fig.8a. SEM images of the grown  $\beta$ -AAP crystals

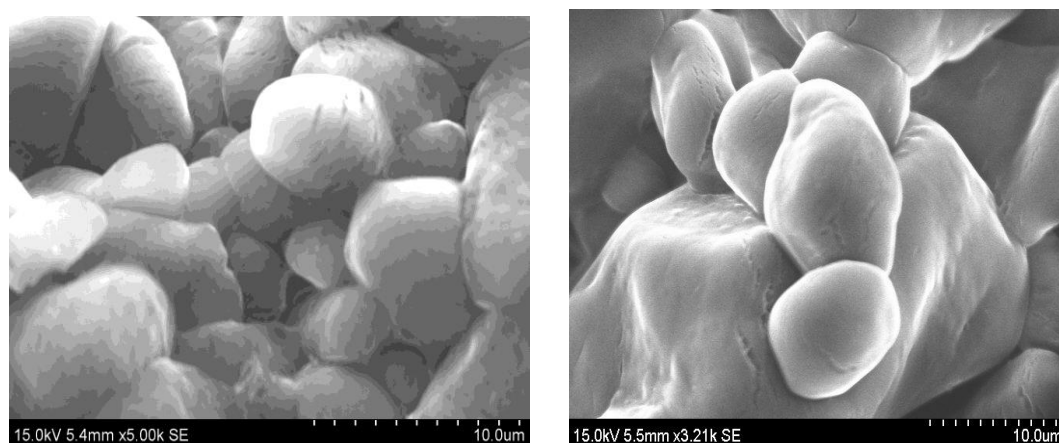


Fig.8b. SEM images of grown  $\beta$ -AAP crystal

### 3.9. Z-SCAN TECHNIQUE

The Z-scan technique is a useful and popular technique for characterizing the third-order optical nonlinearity of the materials [18, 19]. The open and closed aperture Z-scan methods are used for the measurements of non-linear optical refraction and nonlinear absorption coefficient for optical materials. In this technique, Gaussian laser beam is used for molecular stimulation and its propagation direction has been taken as the Z-axis of the optically polished crystal. The beam was focused using a convex lens and the focal point has been taken as  $Z = 0$ . By placing the sample in different positions with respect to the focus of the beam, the corresponding normalized transmission to the crystal was measured. Because of the light induced nonlinearity, the samples transmission will increase or decrease, depending on its Z-position with respect to the focal plane.

The beam will have maximum energy density at the focus which will symmetrically reduce towards either side of it. The nonlinear absorption coefficient ( $\beta$ ) and the nonlinear optical refraction ( $n_0$ ) for the sample have been evaluated from normalized transmission of corresponding Z-position. The monochromatic laser light (1064 nm) from Nd:YAG laser was used for the study. A plane convex lens of 22.5 cm focal length was used to focus the laser beam. The input energy and the energy transmitted by the sample were measured using the power meter. The normalized transmittance for the positioned crystal sample was measured at different positions and was used to calculate third-order nonlinear optical property of the material. The Z-scan technique was employed to investigate the third-order nonlinear optical property of  $\beta$ -AAP single crystal. Z-scan method is based on the principle of spatial beam refraction and offers simplicity as well as very high sensitivity for distinguishing the contribution of real and imaginary part of third-order nonlinear optical susceptibility ( $\chi^{(3)}$ ). The magnitude and sign of the nonlinear refractive index ( $n_2$ ) and the nonlinear absorption coefficient ( $\beta$ ) has been estimated using closed and open aperture mode Z-scan curves [20,21]. From the normalized transmittance curve, it is observed that a peak followed by a valley is the signature for non-linearity of the material [22]. Normalized transmittance in open and closed aperture modes for  $\beta$ -AAP single crystal is shown in Fig. 9 and Fig. 10 respectively. The difference between the normalized peak and valley transmittance is the quantity  $\Delta T_{p,v}$  and was calculated using,

$$\Delta T_{p,v} = 0.406(1 - S)^{0.25} |\Delta \Phi_0| \quad (3)$$

Where  $\Delta \Phi_0$  is the on-axis phase shift at the focus, S is the linear transmittance of aperture and it was calculated using

$$S = 1 - \exp\left(\frac{-2r_a^2}{\omega_a^2}\right) \quad (4)$$

Where  $r_a$  is the radius of aperture and  $\omega_a$  is the spot size diameter in front of the aperture.

The nonlinear refractive index ( $n_2$ ) and the nonlinear absorption coefficient ( $\beta$ ) were determined using

$$n_2 = \frac{\Delta \phi_0}{k I_0 L_{eff}} \quad \text{and} \quad \beta = \frac{2\sqrt{2}\Delta T}{I_0 L_{eff}} \quad (5)$$

where k is the wave number ( $k = 2\pi/\lambda$ ),  $I_0$  is the intensity of the laser beam at the focus ( $Z = 0$ ) and  $L_{eff} = [1 - \exp(-\alpha L)]/\alpha$  is an effective thickness of the sample,  $\alpha$  is the linear absorption coefficient and L is the thickness of the sample and  $\Delta T$  is the normalized transmittance of the sample at position Z. The pure nonlinear refractive index is obtained by dividing the closed aperture transmittance data by the corresponding open aperture transmittance data [23]. The real and imaginary parts of the third-order nonlinear optical susceptibility ( $\chi^{(3)}$ ) were calculated using the equations:

$$\text{Re } \chi^{(3)}(esu) = \frac{10^{-4}(\epsilon_0 C^2 n_0^2 n_2)}{\pi} (cm^2/W) \quad (6)$$

and

$$\text{Im } \chi^{(3)}(esu) = \frac{10^{-2}(\epsilon_0 C^2 n_0^2 \lambda \beta)}{4\pi^2} (cm/W) \quad (7)$$

Where  $\epsilon_0$  is the vacuum permittivity and c is the velocity of light.  $n_0$  is the linear refractive index of the sample and c is the velocity of light in vacuum.

The Z-scan measurements reveal that  $\beta$ -AAP exhibits good third-order nonlinear optical properties such as nonlinear refractive index and nonlinear absorption coefficient. The third order nonlinearity data of the  $\beta$ -AAP crystal is given in Table 2. The nonlinear absorption is attributed to a multi-photon absorption process and the nonlinear refraction leads to the self-defocusing nature of the crystal.

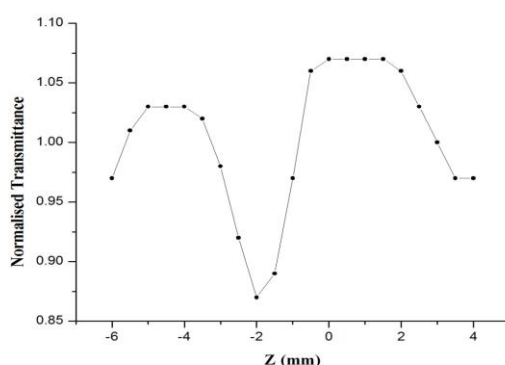


Fig. 9. Open aperture mode Z-scan plot of the  $\beta$ -AAP single crystal.

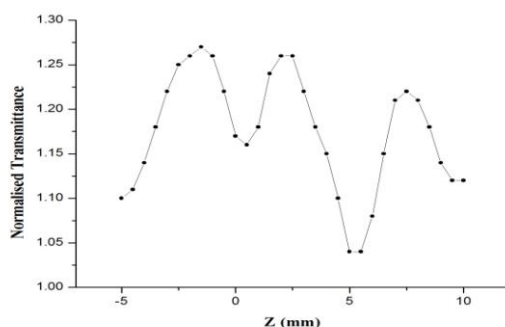


Fig. 10. Closed aperture mode Z-scan plot of the  $\beta$ -AAP single crystal.

Table 2: Obtained data from Z-scan measurements for  $\beta$ -AAP crystal.

Laser beam wave length ( $\lambda$ )	632.8 nm
Lens focal length (f)	18.5 cm / 8.5 cm
Spot size diameter in front of the aperture ( $\omega_a$ )	1cm
Aperture radius ( $r_a$ )	2 mm
Incident intensity at the focus (Z = 0)	3.13 MW/cm <sup>2</sup>
Effective thickness ( $L_{eff}$ )	2.09 mm
Nonlinear refractive index ( $n_2$ )	$5.36 \times 10^{-12}$ cm <sup>2</sup> /W
Nonlinear absorption coefficient ( $\beta$ )	$4.24 \times 10^{-4}$ cm /W
Real part of the third-order nonlinear susceptibility $Re(\chi^{(3)})$	$3.18 \times 10^{-10}$ esu
Imaginary part of the third-order nonlinear susceptibility $Im(\chi^{(3)})$	$1.26 \times 10^{-7}$ esu
The third-order nonlinear optical susceptibility ( $\chi^{(3)}$ )	$3.5 \times 10^{-4}$ esu

#### IV. CONCLUSIONS

Single crystal of  $\beta$ -Alanine  $\beta$ -Alaninium Picrate ( $\beta$ -AAP) was grown by slow evaporation method. The grown crystal was characterized using single crystal X-ray diffraction analysis, which shows that the  $\beta$ -AAP crystal is belong to triclinic system. UV-Vis-NIR study reveals that the  $\beta$ -AAP crystal shows high wide transparency in the entire visible region. The band gap of the  $\beta$ -AAP crystal was found to be 2.1 eV. Various functional groups present in the grown sample were identified by FT-IR analysis. The TGA and DTA studies reveal that the material is thermally stable up to 185° C. The microstructure of the material was analyzed using SEM studies. The relative third order nonlinear optical absorption, the nonlinear optical refractive index and third-order nonlinear optical susceptibility were calculated by the Z-scan technique. The measured third order nonlinear properties confirm its suitability for non-linear optical devices such as optical limiting and switching.

#### REFERENCES

- [1] A. Zamara, K. Rajesh, A. Thirugnanam, P. Praveen kumar, Elsevier-optick, 125, 6082 (2014).
- [2] K. Rajesh, P. Praveen kumar, Hindawi, Journal of Material, Article ID 790957, 5 (2014).
- [3] I. Nemeč, I. Cisarova and Z. Micka, "Nitrate," Journal of Molecular Structure, Vol. 476, No. 1-3, 1999, pp. 243-253. doi:10.1016/S0022-2860(98)00539-0.
- [4] V. D. Gupta and M. V. Krishnan, "Low-Frequency Spectra of L-Alanine," Journal of Physics B: Atomic and Molecular Physics, Vol. 3, No. 4, 1970, p. 572. doi:10.1088/0022-3700/3/4/012.
- [5] D. Philip and G. Aruldas, "Vibrational Spectra of Alanine and Glycine Phosphates," Acta Chimica Academiae Scientiarum Hungaricae, Vol. 127, 1990, pp. 717-723.

- [6] H. Takayanagi, M. K. Goto, K. Takeda and Y. Osa, "X- Ray Crystallographic Analysis of Picrates," Journal of the Pharmaceutical Society of Japan, Vol. 124, No. 11, 2004, pp. 751-767.
- [7] C.Razzetti, M. Ardoino, L. Zanotti, M. Zha and C. Paorici, "Solution Growth and Characterisation of L-Alanine Single Crystals," Crystal Research and Technology, Vol. 37, No.5,2002,pp.456-465.doi:10.1002/1521-4079(200205)37:5<456::AID-RAT456>3.0.CO;2M.
- [8] M.Amudha, J. Madhavan & P. Praveen Kumar, Springer-Journal of Optics. 19 (2016). Doi: 10.1007/s 12596 -016 -0381-y.
- [9] M.A.F. Elmosallamy, Anal. Sci. 20 (2004) 285.
- [10] P.G. Farrell, F. Terrier, R. Schaal, Tetrahedron Lett. 26 (1985) 2435.
- [11] G.C. Franchini, A. Marchetti, L. Tassi, G. Tosi, J. Chem. Soc. 84 (1988) 4427.
- [12] R.C. Maurya, P. Sharma, S. Roy, Synth. React. Inorg. Met. Org. Chem. 33 (2003) 683.
- [13] M. Mohamed Ali Jinnah, M. Umadevi, V. Ramakrishnan, J. Raman Spectrosc. 35 (2004) 956.
- [14] S. Pandi arajan, R.K. Rajaram, V. Ramakrishnan, J. Raman Spectrosc. 36 (2005) 785.
- [15] Bhuvana K. Periyasamy, Robinson S. Jebas, N. Gopalakrishnan, T. Balasubramanian, "Development of NLO tunable band gap organic devices for optoelectronic application," Materials Letters, 61 (21), pp. 4246-4249, (2007).
- [16] N. Tigau, V. Ciupinaa, G. Prodana, G.I. Rusb, C. Gheorghies, E. Vasile, J. Optoelectronics Adv. Mater. (6) 211.
- [17] A.K. Chawla, D.Kaur, R.Chandra, Optical Mater. 29 (2007) 995.
- [18] M. Sheik-Bahae, A.A. Said, E.W. Van Stryland, High-Sensitivity, Single-beam  $n_2$  measurements, Opt. Lett. 14, 955 (1989).
- [19] M. Sheik-Bahae, A.A. Said, T.H. Wei, D.J. Hagan, E.W. Van Stryland, Sensitive Measurement of Optical Nonlinearities using a single beam, IEEE J. Quantum Electron. 26, (1990).
- [20] G. Anandha Babu, P. Ramasamy, spectrochim. Acta A. 82,521 (2011).
- [21] A. Subashini, R. Kumaravel, S. Leela, H.S. Evans, D. Sastikumar, K. Ramamurthi, Spectrochim. Acta A. 78, 935 (2011).
- [22] R. Ranjani, T. Sivanesan, P.R. Umarani, International Journal of ChemTech Research, Vol. 7, 2669 (2015).
- [23] S. Leela, K. Ramamurthi, G. Bhagavannarayana, Spectrochimica, Acta Part A. 7158, 6 (2009).

**FIGURES AND TABLES**

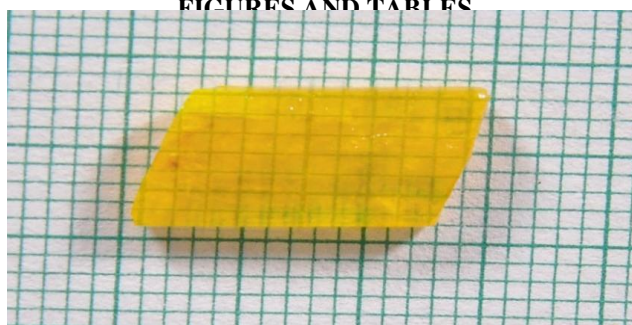


**Fig.1. Photograph of the  $\square$ -AAP crystal.**

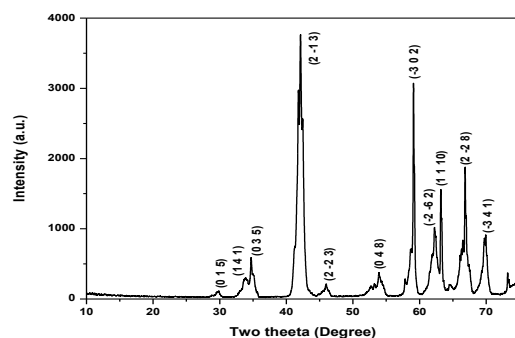


**Fig. 2. Powder XRD spectrum of the  $\square$ -AAP crystal.**

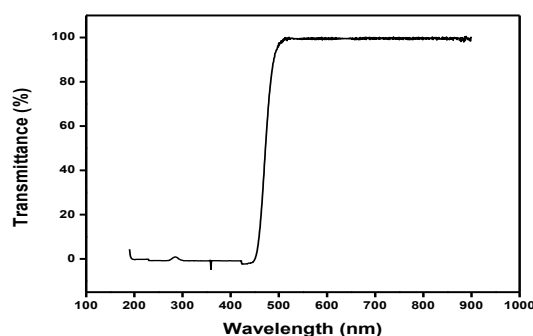


**Fig. 3. UV-Vis-NIR spectra of the  $\square$ -AAP crystal.**

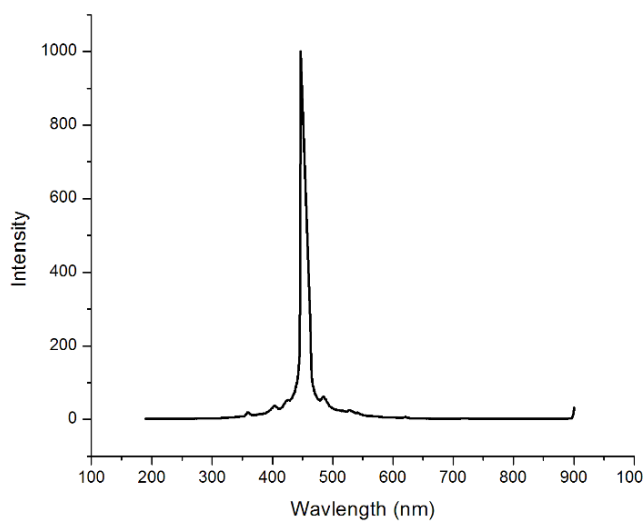


Fig.4. Emission spectrum of the AAP crystal.

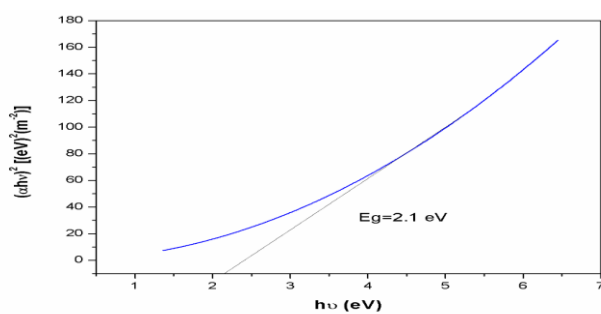


Fig. 5. Plot  $(nh)^2$  Vs  $h\nu$  of the AAP crystal.

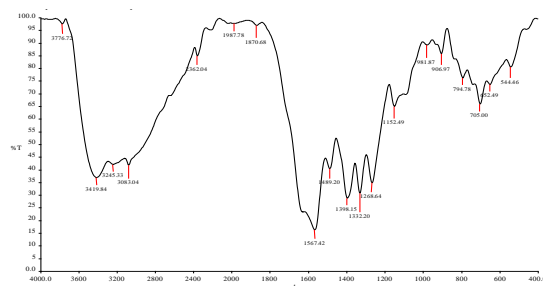


Fig .6.The FT-IR Spectrum of the AAP crystal.

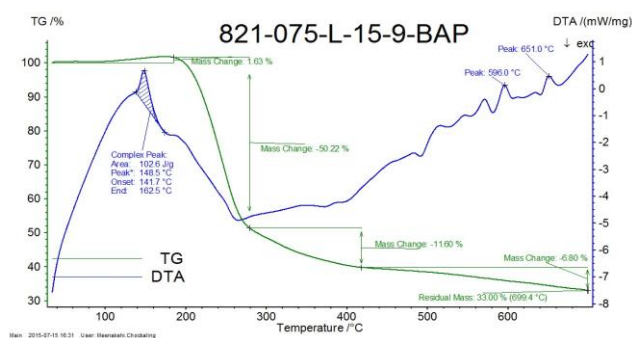


Fig. 7.TG-DTA curves of the AAP crystal.

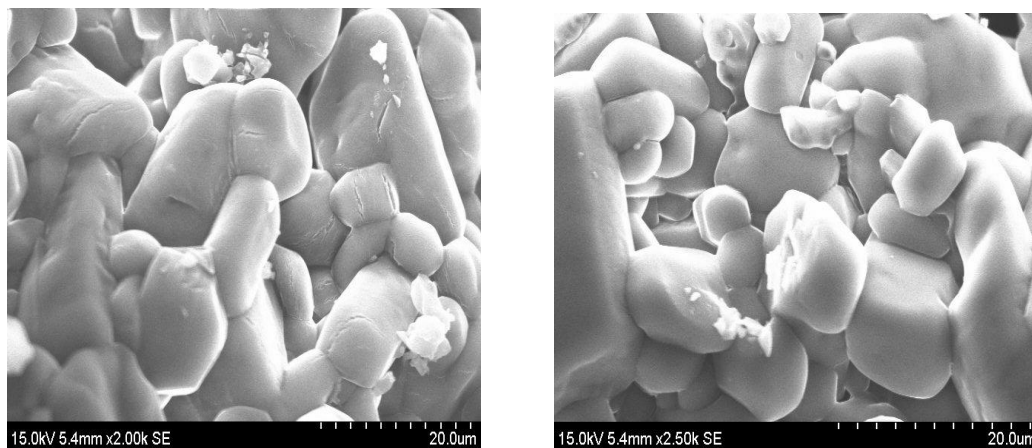


Fig.8a. SEM images of the grown  $\beta$ -AAP crystals

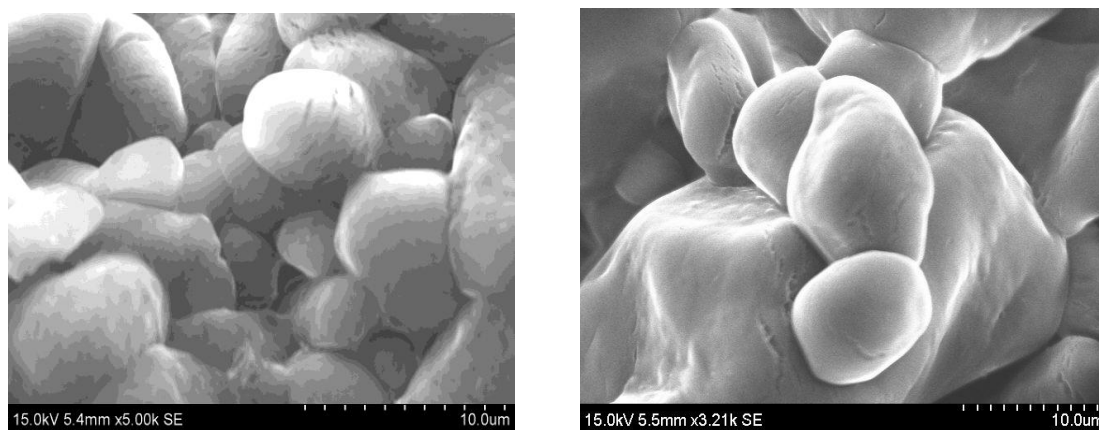


Fig.8b. SEM images of grown  $\beta$ -AAP crystal

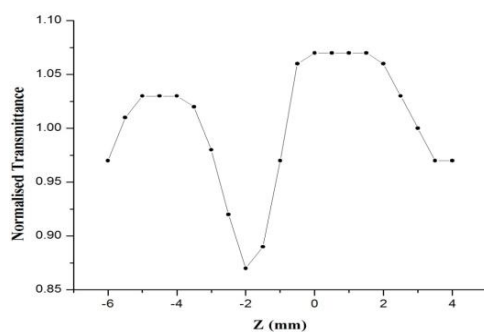


Fig. 9. Open aperture mode Z-scan plot of the  $\beta$ -AAP single crystal.

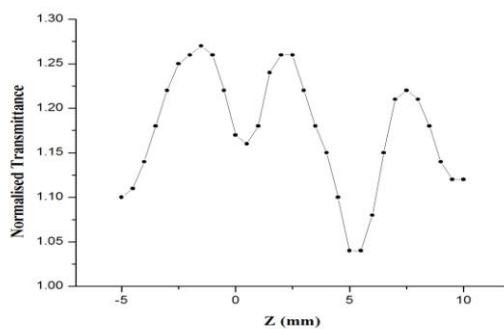


Fig. 10. Closed aperture mode Z-scan plot of the  $\beta$ -AAP single crystal.

**Table:1 FT-IR absorption frequencies of  $\beta$ -AAP crystal.**

Wave number (cm <sup>-1</sup> )	Assignment
3419.84	N-H stretching
3245	Symmetric and asymmetric stretching
3083.04	NH <sub>3</sub> <sup>+</sup> stretching frequencies
1567.42	C=O stretching
1286.64 & 1152.49	C-O stretching
794.78	C-H bending
705.00	C-H stretching

**Table: 2 Obtained data from Z-scan measurements for  $\beta$ -AAP crystal.**

Laser beam wave length ( $\lambda$ )	632.8 nm
Lens focal length (f)	18.5 cm /8.5 cm
Spot size diameter in front of the aperture ( $\omega_a$ )	1cm
Aperture radius ( $r_a$ )	2 mm
Incident intensity at the focus (Z = 0)	3.13 MW/cm <sup>2</sup>
Effective thickness ( $L_{eff}$ )	2.09 mm
Nonlinear refractive index ( $n_2$ )	$5.36 \times 10^{-12} \text{ cm}^2/\text{W}$
Nonlinear absorption coefficient ( $\beta$ )	$4.24 \times 10^{-4} \text{ cm}^2/\text{W}$
Real part of the third-order nonlinear susceptibility $\text{Re}(\chi^{(3)})$	$3.18 \times 10^{-10} \text{ esu}$
Imaginary part of the third-order nonlinear susceptibility $\text{Im}(\chi^{(3)})$	$1.26 \times 10^{-7} \text{ esu}$
The third-order nonlinear optical susceptibility ( $\chi^{(3)}$ )	$3.5 \times 10^{-4} \text{ esu}$